

# Periodic dynamics of population-imbalanced fermionic condensates in optical lattices

Avinaba Mukherjee<sup>1,\*</sup> and Raka Dasgupta<sup>1,†</sup>

<sup>1</sup>*Department of Physics, University of Calcutta, 92 A. P. C. Road, Kolkata 700009, India*

(Dated: January 15, 2024)

We investigate the dynamics of a population-imbalanced two-species fermionic system trapped in an optical lattice. The paired fermions here can form bosonic molecules via Feshbach coupling in the presence of an external magnetic field. It is shown that the natural fluctuations of the condensate fraction are periodic beyond a threshold Feshbach detuning; and below this threshold value, the condensate fraction shows no oscillation at all. The oscillation frequency vs. detuning curve is linear in nature. The slope and intercept of this line are shown to carry important information about the amount of imbalance present in the system, and the momentum space structure of the exotic phases.

PACS numbers: 71.10Ca, 05.30.-d, 42.50Lc, 37.10Jk

## I. INTRODUCTION

Population-imbalanced ultracold fermionic systems remain an active field of research for the past two decades. While it is known that Feshbach-coupled two-species fermionic gases can demonstrate a BCS-BEC crossover as the effective interaction is varied [1–5], the situation changes if the system resembles a spin-polarized state i.e., one species is more populated than the other. In this case, instead of the weakly interacting homogeneous BCS state (that demands both species to be equally populated), one would have novel pairing structures that can accommodate the unpaired fermions. Several theoretically proposed phases exist for such systems, including (i) Breached pair (BP) [6–14] (ii) Phase separation (PS) [15–17] and (iii) Fulde-Ferrell-Larkin-Ovchinnikov (FFLO) states [18–23]. A new phase with a non-FFLO spatially modulated pairing state has also been reported recently [24].

The tunability associated with the ultracold atomic systems went a step ahead with the advent of optical lattices [25–28] as now the geometry as well as the dimension of the lattice could be easily controlled by using the laser beams. As fermionic superfluidity could now be realized in the optical lattices [5, 29, 30], it opened up the possibility of studying the non-BCS exotic pairing phases in the presence of the lattice potentials [31–44]. However, it is extremely difficult to find direct experimental signatures of the theoretically predicted exotic phases (except the PS state [17]), and a few indirect methods has been proposed in the past [12, 45–53].

The study of the out-of-equilibrium dynamics and fluctuation dynamics of ultracold atoms is both an interesting and challenging field [54], because of the in-built nonlinearity of the systems. Oscillatory dynamics of atoms in optical lattices have been probed in the context of Bloch oscillations [55, 56], Collective oscillations [57–66], Josephson junction arrays [67] and spin imbalance dynamics in the presence of superexchange interactions [54, 68]. Most of these involve population oscillations between either two quantum states or two bands. Quantum transport-related properties of ultracold atoms in optical lattices have been studied as well [69–74], where the system is intrinsically non-equilibrium, with al-

most no equilibrium counterpart being present. In this work, however, we start from the equilibrium configurations of the population-imbalanced systems, and explore the fluctuation dynamics on top of it. It is observed that an oscillatory pattern arises in these fluctuations, even at the mean-field level.

In this paper, we study the mean-field level fluctuation dynamics of the population-imbalanced fermionic condensate in an optical lattice for 1D, 2D and 3D. We observe that the dynamics is periodic, and the oscillation frequency changes almost linearly with a varying Feshbach detuning. We can obtain information about the amount of population imbalance present in the system, and also the nature of the pairing, from the slope and intercept of this straight line.

The paper is organized as follows. The basic theoretical model and the dynamical equations are described in Sec. II. In Sec. III, possible pairing phases are discussed and the relevant parameters are set up in different dimensions. The frequency vs. detuning plots are presented in Sec. IV, and it is shown that the oscillation dynamics are periodic. How the intercept of the frequency vs. detuning curve varies with the amount of population imbalance is discussed in Sec. VA, and the same for the slope is done in Sec. VB. In Sec. VI, we provide the analytical reasoning for the numerical results of the previous two sections. The results are summarized in Sec. VII.

## II. MODEL HAMILTONIAN AND DYNAMICS

Here we consider a system of ultracold fermionic atoms in an optical lattice, that can form a bosonic molecule by means of Feshbach resonances. The system can be described by an extended version of the Hubbard Hamiltonian

$$\begin{aligned}
 H = & -t \sum_{\langle \vec{j}\vec{l} \rangle} (a_{\vec{j}\uparrow}^\dagger a_{\vec{l}\uparrow} + a_{\vec{j}\downarrow}^\dagger a_{\vec{l}\downarrow}) - \sum_{\vec{j}} (\mu_\uparrow a_{\vec{j}\uparrow}^\dagger a_{\vec{j}\uparrow} + \mu_\downarrow a_{\vec{j}\downarrow}^\dagger a_{\vec{j}\downarrow}) \\
 & + g_1 \sum_{\vec{j}} n_{\vec{j}\uparrow} n_{\vec{j}\downarrow} + g_2 \left( \sum_{\vec{j}} b_{\vec{j}}^\dagger a_{\vec{j}\downarrow} a_{\vec{j}\uparrow} + \sum_{\vec{j}} a_{\vec{j}\uparrow}^\dagger a_{\vec{j}\downarrow}^\dagger b_{\vec{j}} \right) \\
 & + [\epsilon_b - (\mu_\uparrow + \mu_\downarrow)] \sum_{\vec{j}} b_{\vec{j}}^\dagger b_{\vec{j}} \quad (1)
 \end{aligned}$$

Here, up-spin ( $\uparrow$ ) and down-spin ( $\downarrow$ ) represent either two different atomic species or two different hyperfine states of the same atom;  $\mu_\uparrow$  and  $\mu_\downarrow$  are their respective chemical potentials. The hopping amplitude (assumed to be the same for both species) is  $t$ . Also,  $a_j^\dagger$  and  $a_j$  are respectively the fermionic atom creation and annihilation operators for site  $\vec{j} = (j_x, j_y, j_z)$ , and their bosonic counterparts for molecule creation and destruction are given by  $b_j^\dagger$  and  $b_j$ . The number operators for up-spin and down-spin fermions at  $\vec{j}$ th site are  $n_{j\uparrow}$  and  $n_{j\downarrow}$  respectively. The on-site interaction strength is  $g_1$ , while  $g_2$  is the additional interaction strength of the Feshbach variety which couples two fermionic atoms to form a bosonic molecule. The threshold energy of the composite bosonic molecule energy band is  $\epsilon_b$ , and it is the pivotal adjustable ‘‘detuning’’ parameter in this model.

This Hamiltonian takes the following form in momentum space :

$$\begin{aligned}
H = & \sum_{\vec{k}} \epsilon_{\vec{k}\uparrow} a_{\vec{k}\uparrow}^\dagger a_{\vec{k}\uparrow} + \sum_{\vec{k}} \epsilon_{-\vec{k}\downarrow} a_{-\vec{k}\downarrow}^\dagger a_{-\vec{k}\downarrow} \\
& + g_1 \sum_{\vec{k}, \vec{k}'} a_{\vec{k}\uparrow}^\dagger a_{-\vec{k}+\vec{q}\downarrow}^\dagger a_{-\vec{k}'+\vec{q}\downarrow} a_{\vec{k}'\uparrow} \\
& + g_2 \left( \sum_{\vec{q}, \vec{k}} b_{\vec{q}}^\dagger a_{-\vec{k}+\vec{q}\downarrow} a_{\vec{k}\uparrow} + \sum_{\vec{k}, \vec{q}} a_{\vec{k}\uparrow}^\dagger a_{-\vec{k}+\vec{q}\downarrow}^\dagger b_{\vec{q}} \right) \\
& + [\epsilon_b - (\mu_\uparrow + \mu_\downarrow)] \sum_{\vec{q}} b_{\vec{q}}^\dagger b_{\vec{q}}
\end{aligned} \quad (2)$$

$\epsilon_{\vec{k}\uparrow} = -2t(\cos \vec{k}\vec{a}) - \mu_\uparrow$  and  $\epsilon_{-\vec{k}\downarrow} = -2t(\cos \vec{k}\vec{a}) - \mu_\downarrow$  are the energy-momentum dispersion relation for up-spin and down-spin respectively. Here,  $\vec{a}$  is the lattice vector of the optical lattice. Also,  $a_{\vec{k}\uparrow}^\dagger, a_{\vec{k}\uparrow}$  are the creation and annihilation operators corresponding to momentum  $k$  for one fermionic species, and  $a_{\vec{k}\downarrow}^\dagger, a_{\vec{k}\downarrow}$  are the corresponding operators for the other fermionic species. The bosonic molecule creation and annihilation operators in the momentum space are given by  $b_{\vec{q}}^\dagger$  and  $b_{\vec{q}}$  respectively. Here  $\vec{q}$  is the momentum of the composite bosons and has a magnitude zero for BCS-type of pairing, and a non-zero magnitude if an exotic pairing structure like FFLO is involved. More details about these pairing phases are discussed in **III B**.

We define

$$O_{\vec{k}, \vec{q}} = \langle a_{-\vec{k}+\vec{q}\downarrow} a_{\vec{k}\uparrow} \rangle \quad (3)$$

The equilibrium conditions are given by

$$\frac{\partial O_{\vec{k}, \vec{q}}^{eq}}{\partial t} = 0 \quad \text{and} \quad \frac{\partial b_{\vec{q}}^{eq}}{\partial t} = 0 \quad (4)$$

Now, we consider the intrinsic and spontaneous quantum fluctuations on top of the equilibrium base states. We write,  $O_{\vec{k}, \vec{q}} = O_{\vec{k}, \vec{q}}^{eq} + \tilde{O}_{\vec{k}, \vec{q}}$  and  $b_{\vec{q}} = b_{\vec{q}}^{eq} + \tilde{b}_{\vec{q}}$ . Here,  $b_{\vec{q}}^{eq}$  and  $O_{\vec{k}, \vec{q}}^{eq}$  are the equilibrium value of  $b_{\vec{q}}$  and  $O_{\vec{k}, \vec{q}}$  respectively.

$\tilde{O}_{\vec{k}, \vec{q}}$  is the fluctuation in  $O_{\vec{k}, \vec{q}}$  and  $\tilde{b}_{\vec{q}}$  is the fluctuation in  $b_{\vec{q}}$ . The scheme resembles the one used in [53] for studying population-imbalanced uniform systems as well as trapped systems under local density approximation. Here we extend that scheme to incorporate the effects of optical lattices that are more relevant for present-day experiments.

By calculating the commutation relations of  $b_{\vec{q}}$  and  $O_{\vec{k}, \vec{q}}$  respectively with the Hamiltonian, and imposing the equilibrium conditions, we arrive at two dynamical equations :

$$i\hbar \frac{\partial \tilde{O}_{\vec{k}, \vec{q}}}{\partial t} = \sum_{\vec{k}} (\epsilon_{\vec{k}\uparrow} + \epsilon_{-\vec{k}+\vec{q}\downarrow}) \tilde{O}_{\vec{k}, \vec{q}} - (g_1 \sum_{\vec{k}} \tilde{O}_{\vec{k}, \vec{q}} + g_2 \tilde{b}_{\vec{q}}) \quad (5)$$

$$i\hbar \frac{\partial \tilde{b}_{\vec{q}}}{\partial t} = g_2 \sum_{\vec{k}} \tilde{O}_{\vec{k}} + (\epsilon_b - (\mu_\uparrow + \mu_\downarrow)) \tilde{b}_{\vec{q}} \quad (6)$$

By taking the Fourier transform of Eqs. (5, 6), we obtain

$$\sum_{\vec{k}} \tilde{O}_{\vec{k}, \vec{q}}(\omega) = \frac{g_2 \tilde{b}_{\vec{q}}(\omega) f_1(\omega)}{1 - g_1 f_1(\omega)} \quad (7)$$

Here

$$f_1(\omega) = \sum_{\vec{k}} \frac{1}{\epsilon_{\vec{k}\uparrow} + \epsilon_{-\vec{k}+\vec{q}\downarrow} + \hbar\omega} \quad (8)$$

By putting Eq. (7) in Eq. (6) we get

$$b_{\vec{q}}(\omega) \left( \epsilon_b + \hbar\omega + \frac{g_2^2 f_1(\omega)}{1 - g_1 f_1(\omega)} \right) = 0 \quad (9)$$

Thus, in the Fourier expansion of  $b_{\vec{q}}(t)$ , only those  $b_{\vec{q}}(\omega)$  would survive for which

$$\epsilon_b + \hbar\omega + \frac{g_2^2 f_1(\omega)}{1 - g_1 f_1(\omega)} = 0 \quad (10)$$

Therefore, if there is a single solution of  $\omega$  for Eq. (10), then  $b_{\vec{q}}(t) = b_{\vec{q}}^{eq} + b_1 e^{i\omega t}$  and the condensate fraction ( $|b_{\vec{q}}(t)|^2$ ) would show an oscillatory dynamics with frequency  $\pm\omega$ . If there are two solutions  $\omega_1$  and  $\omega_2$ :  $b_{\vec{q}}(t) = b_{\vec{q}}^{eq} + b_1 e^{i\omega_1 t} + b_2 e^{i\omega_2 t}$ . So, the condensate fraction has three periodic components:  $\pm\omega_1, \pm\omega_2, \pm(\omega_1 - \omega_2)$  and similarly for higher number of allowed  $\omega$  values. If no real solution is found for Eq. (10), then the condensate fraction would have no oscillatory dynamics at all. On the BEC side, these essentially are the Bogoliubov modes of oscillation [75].

As evident from Eq. (8), the quantity  $f_1(\omega)$  involves a sum over all paired regions in the momentum space and is dependent on (i) the dimension of the system, (ii) the amount of population imbalance present in the system, and (iii) the nature of pairing. Thus, the solution for  $\omega$  obtained from Eq. (10), which translates into the frequency of oscillation of the condensate fraction, would contain information about these factors as well.

### III. DIFFERENT VARIANTS OF THE POPULATION IMBALANCED SYSTEM

#### A. Dimension of the system

Most ultracold-atomic experiments offer tremendous flexibility when it comes to the dimensionality of the system. For example, a 1-dimensional (1D) optical lattice can be formed when the potential is shallower in one direction but it is much deeper in the other two directions [76–79]. Converting the summation in Eq. (8) to an integral,

$$f_1(\omega) = \frac{L}{2\pi\hbar} \int \frac{dk}{\epsilon_{\vec{k}\uparrow} + \epsilon_{-\vec{k}+\vec{q}\downarrow} + \hbar\omega} \quad (11)$$

Here  $\epsilon_{\vec{k}\uparrow} = -2t(\cos ka) - \mu_\uparrow$ ,  $\epsilon_{-\vec{k}\downarrow} = -2t(\cos ka) - \mu_\downarrow$ .  $L$  is the quantization length of the optical lattice. Similarly, a 2-dimensional (2D) optical lattice can be formed when the potential is deeper in one direction but shallower in the other two directions [80].

$$f_1(\omega) = \frac{A}{(2\pi\hbar)^2} \int \frac{kdkd\theta}{\epsilon_{\vec{k}\uparrow} + \epsilon_{-\vec{k}+\vec{q}\downarrow} + \hbar\omega} \quad (12)$$

In this case,  $\epsilon_{\vec{k}\uparrow} = -2t(\cos k_x a + \cos k_y a) - \mu_\uparrow$ ,  $\epsilon_{-\vec{k}\downarrow} = -2t(\cos k_x a + \cos k_y a) - \mu_\downarrow$  and  $A$  is the quantization area of the optical lattice.

In 3-dimensional (3D) optical lattices, the potential depths are comparable in three possible directions [81]. Here,

$$f_1(\omega) = \frac{V}{(2\pi\hbar)^3} \int \frac{k^2 \sin\theta dk d\theta d\phi}{\epsilon_{\vec{k}\uparrow} + \epsilon_{-\vec{k}+\vec{q}\downarrow} + \hbar\omega} \quad (13)$$

In this case,  $\epsilon_{\vec{k}\uparrow} = -2t(\cos k_x a + \cos k_y a + \cos k_z a) - \mu_\uparrow$ ,  $\epsilon_{-\vec{k}\downarrow} = -2t(\cos k_x a + \cos k_y a + \cos k_z a) - \mu_\downarrow$  and  $V$  is the quantization volume of the optical lattice. In Eqs. (12) and (13), it is assumed that the lattice constant is the same value in all directions.

#### B. Possible pairing phases

If a system has a population imbalance between the up-spin and down-spin fermions, then different exotic phases arise, because the pairing cannot entirely take place in the BCS way. The phases that we consider here are (i) Breached-Pair-1 state (BP1) or Sarma phase (ii) Breached pair-2 state (BP2) (iii) phase separation (PS), and (iv) FFLO. Fractional imbalance is defined as  $P = \frac{n_\uparrow - n_\downarrow}{n_\uparrow + n_\downarrow}$ . Here,  $n_\uparrow$  and  $n_\downarrow$  stand for number of up-spin and down-spin respectively.

In Fig. 1, the blue region and the red dashed regions indicate the paired and unpaired region respectively for a one-dimensional Fermi gas, and different types of pairing structures are depicted. Breached pair or Sarma phase appears at  $T = 0$ ,  $\Delta \neq 0$ ,  $P \neq 0$  (here,  $\Delta$  is the energy gap). In the BP1 (Fig. 1 (a)) structure for a 1-dimensional system, we get the paired region near the ends of the momentum-space

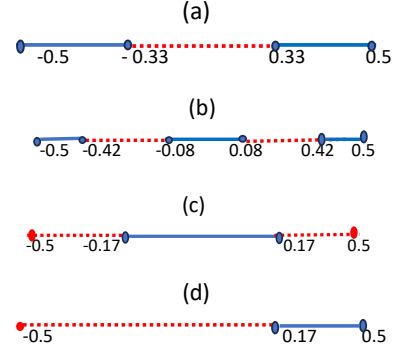


FIG. 1. The structure of different pairing phases in population imbalanced fermionic systems in unit of  $\pi$  for 1D of (a) BP1 (b) BP2 (c) PS (d) FFLO: Blue and red indicates paired and unpaired region at  $P = 0.5$

line, and the unpaired free fermi gas remains in the middle. In BP2 (Fig. 1 (b)) structure for 1-dimension, we get the paired region at both ends of the line and also in the middle, and the “breached” regions with a single species exist in-between. Phase separation (Fig. 1 (c)) is defined as the coexistence of superfluid ( $\Delta \neq 0$ ,  $P = 0$ ) and normal states ( $\Delta = 0$ ,  $P \neq 0$ ). In Fig. 1 (c), the paired region expands about  $k = 0$ . FFLO (Fig. 1 (d)) state is a BCS-like paired state but with a non-zero total momentum. FFLO state is not translationally invariant like BCS and BP phases. Here, the gap parameter is  $\Delta(r) = \Delta e^{2iq\cdot\vec{r}}$  ( $q > 0$ ) where  $\vec{r}$  is the distance from the origin. Out of these phases, BP1, BP2 and FFLO involve specific structures in momentum space. Although these phases have been predicted long back, direct experimental signatures of these phases are difficult to obtain. In contrast, phase separation appears in real space, and is easier to identify experimentally [17]. Here the value of  $f_1(\omega)$  in Eq. (10) has to be evaluated by using Eq. (11). The limit of the integration is chosen in accordance with the structure of the pairing phases as shown in Fig. 1. As an example, for fractional imbalance,  $P = 0.5$ , we put the limits of the  $k$  value of the paired region as  $k = -0.5\pi$  to  $k = -0.33\pi$  and  $k = 0.33\pi$  to  $k = 0.5\pi$  for BP1. The paired region in BP2 is taken as  $k = -0.5\pi$  to  $k = -0.42\pi$ ,  $k = -0.08\pi$  to  $k = 0.08\pi$  and  $k = 0.42\pi$  to  $k = 0.5\pi$ . The paired region in PS spans from  $k = -0.17\pi$  to  $k = 0.17\pi$ . In FFLO, the paired region is  $k = 0.17\pi$  to  $k = 0.5\pi$ . The signature of different pairing phases (BP1, BP2, PS, FFLO) is depicted in terms of total energy ( $\epsilon_{total}$ ) and momentum ( $k$ ) dispersion diagram in Fig. 2. Here,  $\epsilon_{total}$  is the total energy of up-spins and down-spins for the paired region and only up-spins in the unpaired region. In 2D or 3D, the BP1 (Fig. 3) is a two-shell structure of the free fermi gas and the superfluid in momentum space. The BP2 state (Fig. 4) in 2D and 3D is a three-shell structure of the free fermi gas and the superfluid in momentum space. In Fig. 5, the nature of FFLO pairing is depicted where there is the non-zero momentum pairing between red (up-spin) and blue atoms (down-spin) [82] in 2D. The phase-separated state, on the other hand, originates when the up-spin (red) and down-

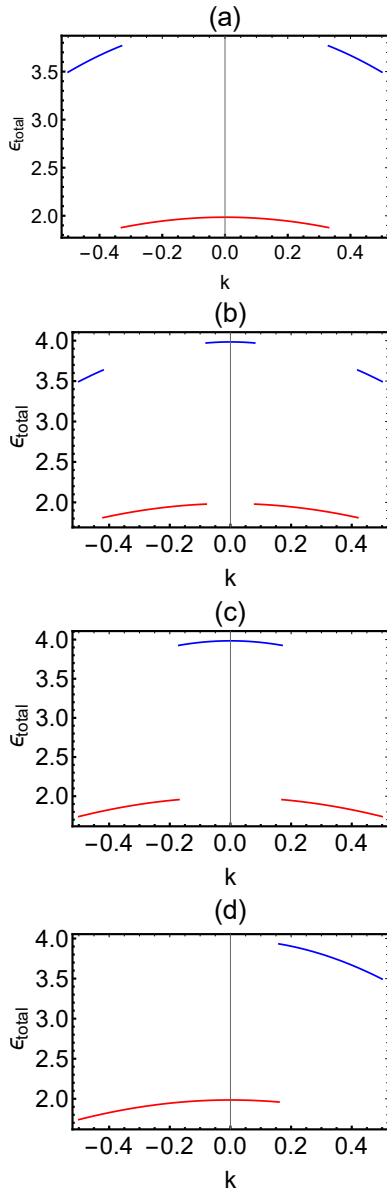


FIG. 2. Total energy ( $\epsilon_{total}$ ) - momentum ( $k$ ) dispersion diagram for 1D of (a) BP1 (b) BP2 (c) PS (d) FFLO at  $P = 0.5$ : Blue and red indicates paired and unpaired region, here momentum in unit of  $\pi$ .

spin (blue) atoms pair with each other and repel the redundant atoms [83], leading to a phase separation between the paired superfluid fermions and the excess unpaired fermions (as shown in Fig. 6).

The integration limits for solving Eqs. (12) and (13) numerically in later sections have been chosen in accordance with the pairing structures described here, and are elaborated further in IV.

### C. System parameters

In this subsection, we set up the parameter values for different types of pairing structures to numerically solve Eq. (10). We choose the following values for the optical lattice depth:  $V_x = 6E_R^F$  and  $V_y = V_z = 40E_R^F$  for 1D;  $V_x = V_y = 6E_R^F$  and  $V_z = 40E_R^F$  for 2D; and  $V_x = V_y = V_z = 6E_R^F$  for 3D. Here  $E_R^F$  is the recoil Fermi energy. The wavelength of the laser beam that creates the optical lattice is chosen to be  $\lambda = 825$  nm as in [84]. In  $x$  direction the hopping amplitude is given by [30, 84–91]

$$\frac{t}{E_R^F} = \frac{4}{\sqrt{\pi}} \left( \frac{V_x}{E_R^F} \right)^{\frac{3}{4}} e^{-2\sqrt{V_x/E_R^F}} \quad (14)$$

Hopping in  $y$  and  $z$  directions can be calculated in a similar fashion. The interatomic coupling  $g_1$  is given by [90]

$$g_1 = \sqrt{\frac{8}{\pi}} k a_{bg} E_R^F \left( \frac{V_x}{E_R^F} \right)^{\frac{1}{4}} \left( \frac{V_y}{E_R^F} \right)^{\frac{1}{4}} \left( \frac{V_z}{E_R^F} \right)^{\frac{1}{4}} \quad (15)$$

The background scattering length ( $a_{bg}$ ) for different fermionic species ( $^6\text{Li}$  and  $^{40}\text{K}$ ) are given in Table I. If the optical lattice potential is quite deep ( $\geq 5E_R^F$ ), only the lowest two energy bands remain relevant. In this case, the additional interaction in the form of Feshbach coupling is given by,

$$g_2 = \sqrt{\frac{4\pi\hbar^2 a_{bg} \Delta B \mu_{co}}{m_F}} \left( \int dx \mathcal{W}_x^B [\mathcal{W}_x^F]^2 \int dy \mathcal{W}_y^B [\mathcal{W}_y^F]^2 \int dz \mathcal{W}_z^B [\mathcal{W}_z^F]^2 \right) \quad (16)$$

Here  $\mathcal{W}_x^B$ ,  $\mathcal{W}_y^B$ ,  $\mathcal{W}_z^B$  are Wannier functions for bosons along  $x$ ,  $y$ ,  $z$  direction respectively, and  $\mathcal{W}_x^F$ ,  $\mathcal{W}_y^F$ ,  $\mathcal{W}_z^F$  are their fermionic counterparts [92]. Again, for sufficiently deep lattice potentials, the Wannier functions can be approximated by harmonic oscillator wavefunctions. For  $x$ -direction, we thus take the bosonic Wannier function to be

$$\mathcal{W}_x^B = \left( \frac{m_B \omega_x^B}{\pi \hbar} \right)^{\frac{1}{4}} e^{-(m_B \omega_x^B x^2)/2\hbar} \quad (17)$$

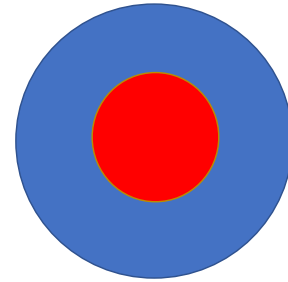


FIG. 3. The momentum-space structure of BP1 phase in 2D: the blue shell contains superfluid and the red region contains free fermi gas

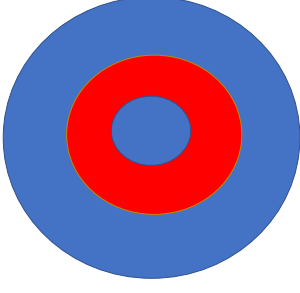


FIG. 4. The momentum-space structure of BP2 phase in 2D : the blue regions contains superfluid and the red region contains free fermi gas

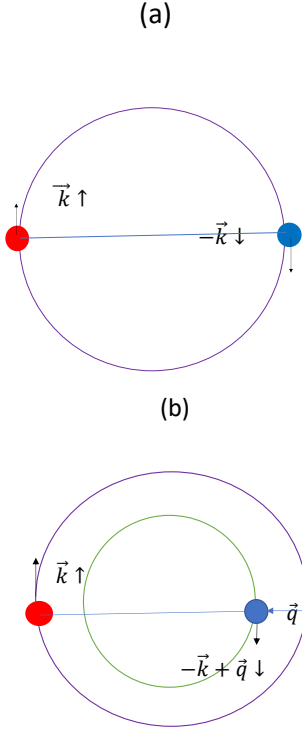


FIG. 5. (a) Usual BCS type of pairing (b) FFLO type of pairing

and fermionic Wannier function to be

$$\mathcal{W}_x^F = \left( \frac{m_F \omega_x^F}{\pi \hbar} \right)^{\frac{1}{4}} e^{-(m_F \omega_x^F x^2)/2\hbar} \quad (18)$$

as in [93]. Here,  $m_B$  and  $m_F$  are the masses of the bosonic molecule and fermionic atoms respectively. In addition, we consider  $\mu_{co} = 2\mu_B$  [94],  $\omega_x^B = \frac{2}{\hbar} \sqrt{V_x E_R^B}$  [95],  $\omega_x^F = \frac{2}{\hbar} \sqrt{V_x E_R^F}$  [95]. Here,  $E_R^B (= \frac{\hbar^2 k^2}{2m_B})$  is the bosonic recoil energy and  $\Delta B$  is the resonance width. Similarly,  $\mathcal{W}_y^F$  and  $\mathcal{W}_z^B$  can be computed from  $V_y$ ; while  $\mathcal{W}_z^F$  and  $\mathcal{W}_z^B$  can be computed from  $V_z$ .

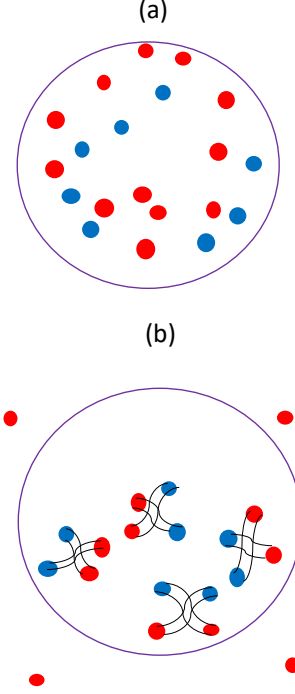


FIG. 6. (a) low attraction strength between red and blue atoms (b) moderate attraction strength between red and blue atoms which generate the phase separation state

Combining all these, the coupling  $g_2$  can be expressed as :

$$g_2 = \sqrt{\frac{4\pi a_{bg} \Delta B \mu_{co}}{m_F \hbar}} \left( \frac{2m_B}{\pi} \right)^{\frac{3}{4}} (E_R^B)^{\frac{3}{8}} (V_x^B V_y^B V_z^B)^{\frac{1}{8}} \left( \frac{2}{2 + \sqrt{\frac{m_B}{m_F}}} \right)^{\frac{3}{2}} \quad (19)$$

$$\epsilon_b = \mu_{co}(B - B_0) \quad (20)$$

Here,  $B_0$  is the Feshbach resonance position and  $B$  indicate applied field.

The complete list of system parameters for 1D, 2D and 3D that we compute, and use for solving the dynamical equations are given in Tables II, III and IV in Appendix A.

#### IV. VARIATION OF FREQUENCY WITH DETUNING

In this section, we present the numerical solutions of Eq. (10) in different dimensions, for different types of pairing structures in a population-imbalanced system. The result is presented in the form of oscillation frequency ( $\omega$ ) of the condensate fraction vs. detuning ( $\epsilon_b$ ) of the Feshbach resonance for two distinct fermionic systems:  $^6\text{Li}$  and  $^{40}\text{K}$ .



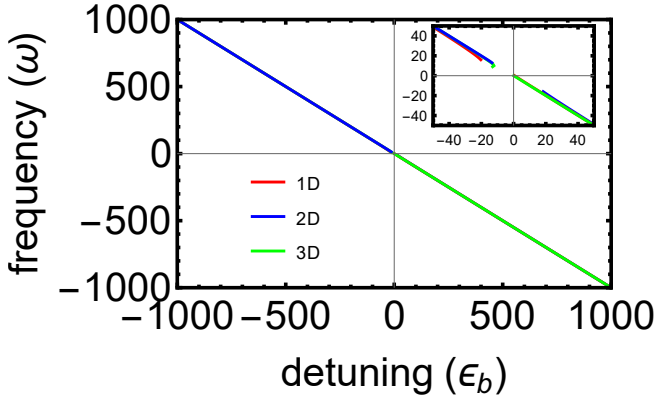


FIG. 7.  $\omega$  vs.  $\epsilon_b$  plot at fractional imbalance  $P = 0.5$  for phase separation of  ${}^6\text{Li}$ : (a) Red for 1D (b) Blue for 2D (c) Green for 3D near narrow resonance. Inset: the enlarged view of the no-oscillation region is indicated by the gap near the resonance point.

### A. Dynamics in 1-dimensional systems

The  $\omega$  vs.  $\epsilon_b$  plots for  ${}^6\text{Li}$  near the narrow resonance (resonance width  $\Delta B = 0.1$  G, resonance position  $B_0 = 543.25$  G) is shown in Fig. 7. Here we find that for all values of  $\epsilon_b$ , (except near  $\epsilon_b = 0$ ) there exists a single value of  $\omega$ . It implies that the dynamics of  $b_{\vec{q}}$  is periodic:

$$b_{\vec{q}}(t) = b_{\vec{q}}^{eq} + b_1 e^{i\omega t} \quad (21)$$

Therefore, the condensate fraction goes as

$$|b_{\vec{q}}(t)|^2 = |b_{\vec{q}}^{eq}|^2 + |b_1|^2 + (b_{\vec{q}}^{eq})^\dagger b_1 e^{i\omega t} + b_1^\dagger b_{\vec{q}}^{eq} e^{-i\omega t} \quad (22)$$

So, essentially it would contain a  $\cos \omega t$  component. Thus, the dynamics of the condensate fraction would be periodic as well.

The  $\omega$  vs.  $\epsilon_b$  curve is almost linear in nature. There is a small region with no real solution for  $\omega$  in the central region (Inset of Fig. 7). It means that no periodic fluctuation is sustained in the dynamics of the condensate fraction for this particular parameter regime. The plot for  ${}^{40}\text{K}$  (resonance width  $\Delta B = 7.8$  G,  $B_0 = 202.10$  G) shows a similar pattern in Fig. 8, but the region with no solution for  $\omega$  is wider. This suggests that the condensate fraction shows no oscillation if the magnitude of the detuning is lower than a threshold value, and there is a periodic oscillation beyond it. The nature of the  $\omega$  vs.  $\epsilon_b$  plots is similar in all possible pairing phases. We would like to mention that the  $\omega$  vs.  $\epsilon_b$  curve for the broad resonance in  ${}^6\text{Li}$  ( $\Delta B = 300$  G,  $B_0 = 834.15$  G) shows similar behaviour. However, the range over which no real solution of  $\omega$  is obtained is much wider in this case, and one gets the straight-line-like curve only when the magnitude of the detuning is very large. For the relatively broader resonance of  ${}^{40}\text{K}$  ( $\Delta B = 9.7$  G,  $B_0 = 224.21$  G), the  $\omega$  vs.  $\epsilon_b$  curve is almost similar to the narrower resonance case. These sets of plots (broad resonances of  ${}^6\text{Li}$  and  ${}^{40}\text{K}$ ) are not included in the present manuscript.

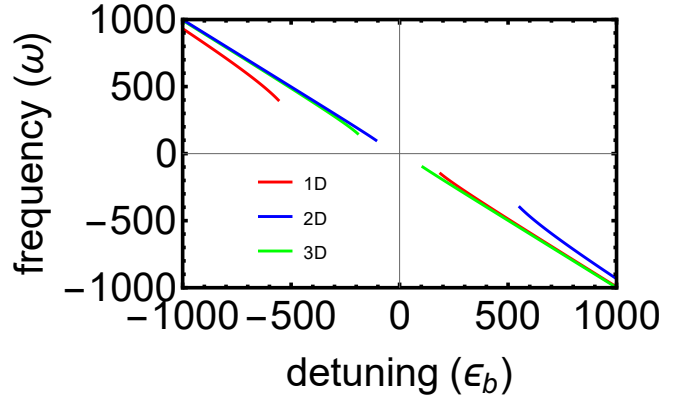


FIG. 8.  $\omega$  vs.  $\epsilon_b$  plot at fractional imbalance  $P = 0.5$  for phase separation in  ${}^{40}\text{K}$  (narrow resonance width): (a) Red for 1D (b) Blue for 2D (c) Green for 3D

### B. Dynamics in 2-dimensional systems

Here, the momentum space phase diagram is a circle. the limits of the integration in Eq. (12) are chosen accordingly. We set the total radius of the circle as unity, i.e., all other momenta are scaled by the Fermi momentum  $k_F$  of the majority species. For fractional imbalance  $P = 0.5$ , we put the limits of the paired region as  $k = 0.82$  to  $1$  for BP1. The paired region in BP2 spans from  $k = 0$  to  $k = 0.41$ , and  $k = 0.91$  to  $1$ . The paired region in PS extends from  $k = 0$  to  $k = 0.58$ . The paired region of FFLO is  $k=0$  to  $k = 0.58$  with shifted origin at  $(0.42, 0)$ .

The  $\omega$  vs.  $\epsilon_b$  curve here looks nearly similar to the 1D case. Only the region for no solution is narrower.

### C. Dynamics in 3-dimensional systems.

The momentum space phase diagram in 3D is a sphere, and we set the total radius of the sphere as unity. As for the limits of the integration in Eq. (13) for fractional imbalance  $P = 0.5$ , the paired region spans from  $k = 0.87$  to  $k = 1$  for BP1, from  $k = 0$  to  $k = 0.55$ , and  $k = 0.94$  to  $k = 1$  for BP2. The paired region spans from  $k = 0$  to  $k = 0.69$  for PS. The paired region in FFLO spans from  $k=0$  to  $0.69$  with shifted origin at  $\{0.69, 0, 0\}$ .

Here, too, we find that for all values of  $\epsilon_b$ , there exists a single value of  $\omega$ , meaning the oscillation of the condensate fraction is periodic as in Eq. (21).

The same trend (i.e., a periodic oscillation except near the resonance point) is observed in this case as well. The span of the region of no solution is less than the corresponding regions in 1D. The  $\omega$  vs.  $\epsilon_b$  curve is almost linear.

Thus, by comparing Figs. 7, and 8 we see that the phase plots do not differ much if the dimension is altered. Also, no major difference vis à vis the choice of the atoms ( ${}^6\text{Li}$  vs.  ${}^{40}\text{K}$ ) is found.

We would like to highlight here that the frequencies of oscillation of the condensate fraction fall well within the experimentally detectable range. If the range of detuning is 5 G to 50 G [96] away from the resonance point ( $B_0 = 543.25$  G [94] for narrow resonance width of  ${}^6\text{Li}$ ), we get the frequency in GHz range for all possible dimensions. As an example, in Figs. 7 and 8 the  $\epsilon_b = 1000$  point in our scale implies a detuning of 1 G apart from the resonance point. The corresponding oscillation frequency is  $\omega = 1000$ . In our convention, this translates to a frequency of 0.019 GHz. In all these numerical computations we set  $\hbar = 1$ .

Additionally, we observe that if the amount of fractional imbalance is changed, then although the qualitative nature of the curves remains the same, some quantitative changes are involved. To quantify these changes, we cast each  $\omega$  versus  $\epsilon_b$  plot in the form

$$\omega = b\epsilon_b + c \quad (23)$$

Here  $b$  and  $c$  are the slopes and intercepts of the line respectively.

In the next section, we report the effects of population imbalance on the intercept ( $c$ ) and slope ( $b$ ) of this  $\omega$  vs.  $\epsilon_b$  plots.

## V. EFFECTS OF POPULATION IMBALANCE

The effective scattering length [97, 98]

$$a_s = a_{bg} \left(1 - \frac{\Delta B}{B - B_0}\right) \quad (24)$$

In Eq. 24  $a_s$ ,  $a_{bg}$ ,  $\Delta B$ , and  $(B - B_0)$  are scattering length, background scattering length, resonance width and applied magnetic field for  $\epsilon_b$  respectively. For the atoms, we consider ( $\text{Li}^6$  and  $\text{K}^{40}$ )  $a_{bg} > 0$ . It is clear that if  $B - B_0 > 0$  i.e  $\epsilon_b > 0$ , and  $\frac{\Delta B}{B - B_0} < 1$  then  $a_s > 0$  which implies BEC. If  $\epsilon_b < 0$ , then  $a_s > 0$  which is also in BEC. We only concentrate on the BEC side for oscillation of condensate fraction.

### A. Variation of intercept with fractional imbalance

In this section, the linearized form of the  $\omega$  vs.  $\epsilon_b$  plot is studied and the intercept is extracted. Here we investigate the effect of the population imbalance on the value of this intercept. The result is presented in the form of intercept ( $c$ ) versus fractional imbalance ( $P$ ) plot for  ${}^6\text{Li}$ . We find that these plots are parabolic in nature.

Fig. 9 shows that if the fractional imbalance increases, then the absolute value of the intercept decreases for all the phases in  ${}^6\text{Li}$  for frequency range  $16 \leq \omega \leq 1000$ .

Fig. 10 shows that if the fractional imbalance increases, then the absolute value of the intercept decreases for different phases in  ${}^6\text{Li}$  for frequency range  $9 \leq \omega \leq 1000$ . Fig. 11 shows that like the 1D and 2D cases the  $c$  vs.  $P$  plot for 3D, too is similar in nature for all possible phases in the frequency

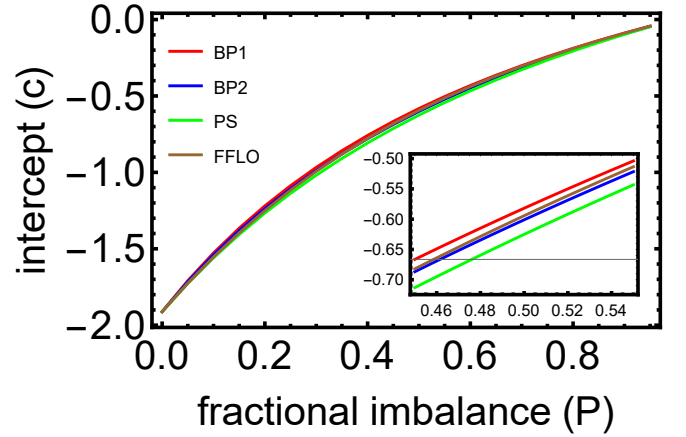


FIG. 9.  $c$  vs.  $P$  plot for various phases in positive frequency and a negative detuning domain of  ${}^6\text{Li}$ : (a) Red for BP1 (b) Blue for BP2 (c) Green for PS (d) Brown for FFLO at narrow resonance width in 1D. Inset: Distinct signature of four novel phases near  $P = 0.5$ .

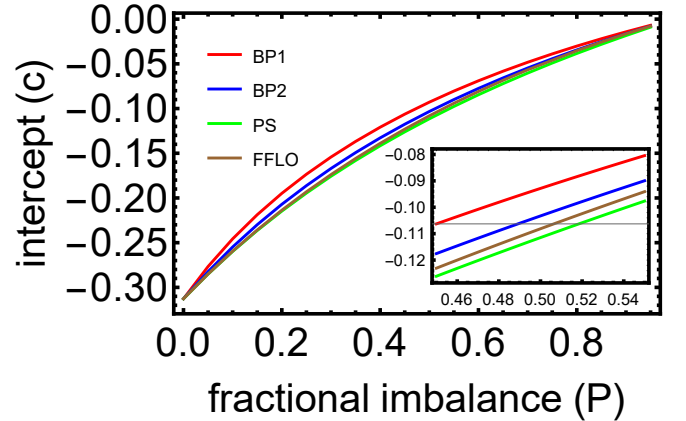


FIG. 10.  $c$  vs.  $P$  plot for various phases in positive frequency and a negative detuning domain of  ${}^6\text{Li}$ : (a) Red for BP1 (b) Blue for BP2 (c) Green for PS (d) Brown for FFLO at narrow resonance width in 2D. Inset: Distinct signature of four novel phases near  $P = 0.5$ .

range  $13 \leq \omega \leq 1000$ .

In the next section, we try to study the effect of  $P$  on the slope ( $b$ ) of the linearized form of the  $\omega$  vs.  $\epsilon_b$  curve.

### B. variation of the slope with population imbalance

In this section, we study how the  $\omega$  vs.  $\epsilon_b$  plots in Sec. IV change with a varying amount of population imbalance. For this, we extract the slope  $b$  from the linearized form of the curves as in Eq. (23). The result is presented in the form of a slope ( $b$ ) versus fractional imbalance ( $P$ ) plot for  ${}^6\text{Li}$ . It appears that these curves are parabolic in nature.

Figs. 12, 13, 14 show that if  $P$  increases then the absolute value of the slope decreases for four phases in  ${}^6\text{Li}$  in 1D ( $16 \leq$

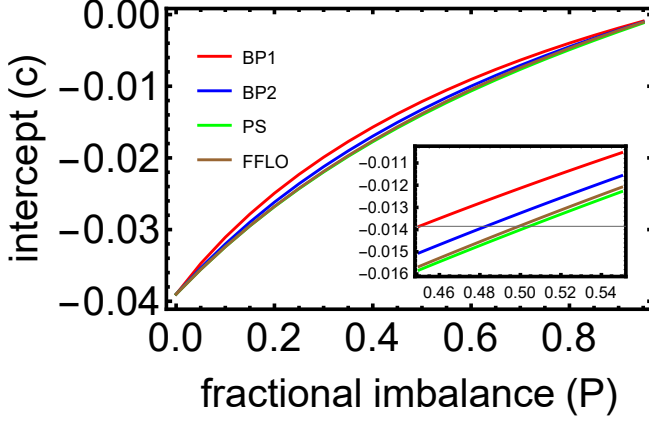


FIG. 11.  $c$  vs.  $P$  plot for various phases in positive frequency and a negative detuning domain of  ${}^6\text{Li}$ : (a) Red for BP1 (b) Blue for BP2 (c) Green for PS (d) Brown for FFLO at narrow resonance width in 3D. Inset: Distinct signature of four novel phases near  $P = 0.5$ .

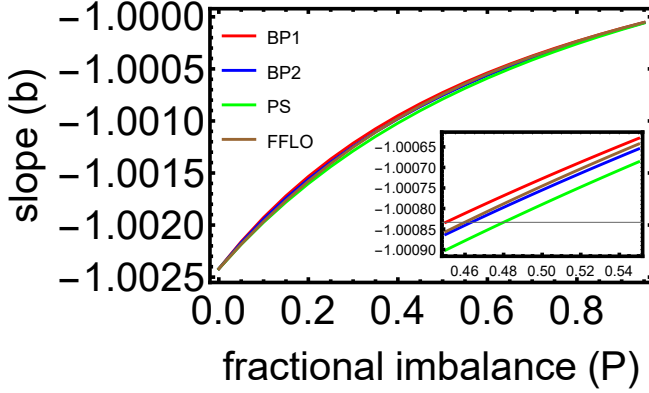


FIG. 12.  $b$  vs.  $P$  plots for various phases in positive frequency and a negative detuning domain of  ${}^6\text{Li}$ : (a) Red for BP1 (b) Blue for BP2 (c) Green for PS (d) Brown for FFLO at narrow resonance width in 1D. Inset: Distinct signature of four novel phases near  $P = 0.5$ .

$\omega \leq 1000$ ), 2D ( $9 \leq \omega \leq 1000$ ), and 3D ( $13 \leq \omega \leq 1000$ ).

It is to be noted that the  $P = 0$  limit corresponds to perfect BCS-type pairing with no population imbalance, and the  $P = 1$  limit corresponds to the presence of a single-fermionic species only. That is why in these two extreme limits, all the phases merge. At the intermediate point ( $P = 0.5$ ) the curves corresponding to different phases are maximally separated from one another.

## VI. ANALYZING THE NATURE OF THE SLOPES AND THE INTERCEPTS

In this section, we try to explain the results presented in [V A](#) and [V B](#), by means of providing analytical arguments and physical justifications. We first establish that there would be

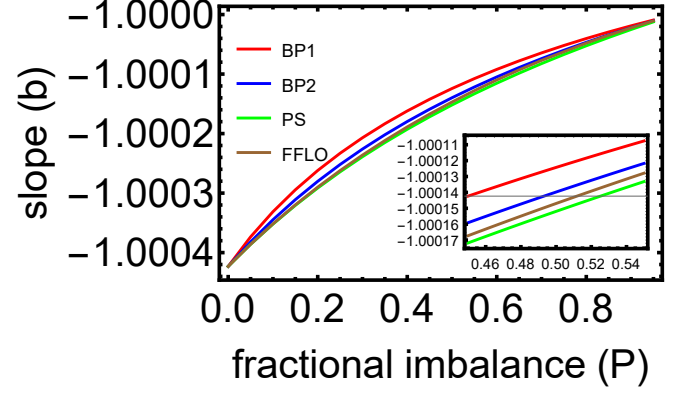


FIG. 13.  $b$  vs.  $P$  plot for various phases in positive frequency and a negative detuning domain of  ${}^6\text{Li}$ : (a) Red for BP1 (b) Blue for BP2 (c) Green for PS (d) Brown for FFLO at narrow resonance width in 2D. Inset: Distinct signature of four novel phases near  $P = 0.5$ .

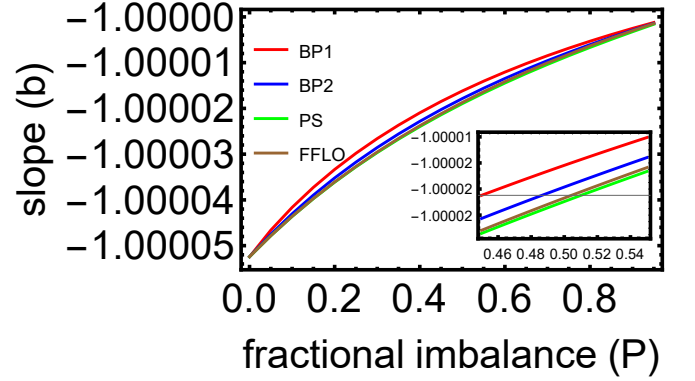


FIG. 14.  $b$  vs.  $P$  plot for various phases in positive frequency and a negative detuning domain of  ${}^6\text{Li}$ : (a) Red for BP1 (b) Blue for BP2 (c) Green for PS (d) Brown for FFLO of at narrow resonance width in 3D. Inset: Distinct signature of four novel phases near  $P = 0.5$ .

only one non-trivial solution for  $\omega$  from Eq. (10). Then we argue that the absolute value of the slope ( $b$ ) and the intercept ( $c$ ) of the  $\omega$  vs.  $\epsilon_b$  curve depends on (i) the amount of imbalance present, and (ii) the exact nature of pairing.

### A. A single branch of $\omega$

We observe that the function  $f_1(\omega)$  can be approximated by a simpler function

$$f_1(\omega) \approx \frac{\alpha}{\hbar\omega}. \quad (25)$$

Here the value of  $\alpha$  depends on (i) the dimension of the system, (ii) the amount of population imbalance present, and (iii) the nature of the pairing. In Fig. 16 we plot  $f_1(\omega)$  and  $\frac{\alpha}{\hbar\omega}$  for 1D to show how close the two functions are. In this plot, the blue solid line and the red dashed line represent  $f_1(\omega)$  and



$\frac{\alpha}{\hbar\omega}$  respectively. So, Eq. (10) will now be

$$\epsilon_b = -\hbar\omega - \frac{g_2^2\alpha}{\hbar\omega - g_1\alpha} \quad (26)$$

Simplifying the above equation we get

$$\omega_{\pm} = \frac{g_1\alpha - \epsilon_b}{2\hbar} \pm \frac{\sqrt{(\epsilon_b - g_1\alpha)^2 - 4\alpha(g_2^2 - g_1\epsilon_b)}}{2\hbar} \quad (27)$$

Thus, we obtain two roots. One root is close to zero and the other root is non-trivial. For positive  $\epsilon_b$  values, we have  $\omega_- \gg \omega_+$  and  $\omega_+ \approx 0$ . Similarly, For negative  $\epsilon_b$  values,  $\omega_+ \gg \omega_-$  and  $\omega_- \approx 0$ . Thus, only one significant solution for  $\omega$  exists, and that explains the nature of the plots in Figs. 7, and 8. Therefore, the condensate fraction's fluctuation is purely periodic as in Eq. (22).

There exists no real root for  $\omega$  if

$$\frac{g_1g_2\alpha + 2\sqrt{\alpha}g_2^2}{g_2 + \sqrt{\alpha}g_1} > \epsilon_b > -\frac{g_1g_2\alpha + 2\sqrt{\alpha}g_2^2}{g_2 + \sqrt{\alpha}g_1} \quad (28)$$

Then, one gets an imaginary frequency solution. Now,  $\Delta\epsilon_b = 2\left(\frac{g_1g_2\alpha + 2\sqrt{\alpha}g_2^2}{g_2 + \sqrt{\alpha}g_1}\right)$ , is the range of that detuning which yields imaginary frequency solution. From Table [V], we observe that  $\alpha_{PS} > \alpha_{FFLO} > \alpha_{BP2} > \alpha_{BP1}$ . So, we get  $(\Delta\epsilon_b)_{PS} > (\Delta\epsilon_b)_{FFLO} > (\Delta\epsilon_b)_{BP2} > (\Delta\epsilon_b)_{BP1}$ .

## B. Effect of the population imbalance on the slope and intercept of $\omega$ vs. $\epsilon_b$ curves

The limits of the integration in Eqs. (11), (12) and (13) are controlled by the fractional imbalance  $P$ . So,  $f_1(\omega)$  depends on  $P$ . If  $f_1(\omega)$  is approximated as in Eq. (25), we find that if  $P$  decreases, then  $\alpha$  increases and vice versa. A set of  $\alpha$  vs.  $P$  values is presented in Table [VI] for the PS state, and the overall trend remains the same for the other phases as well.

### 1. Variation of intercept ( $c$ ) with fractional imbalance ( $P$ )

The  $\omega_+$  vs.  $\epsilon_b$  curve for  ${}^6\text{Li}$  (narrow resonance width) at  $P = 0.5$ , as obtained from Eq. (27) is presented in Fig. 15, corresponding to  $\epsilon_b > 0$  and PS state in 1D. It clearly indicates a positive intercept, i.e.,  $c > 0$ . It can be argued that if  $\omega_- \approx 0$  in Eq. (27), then

$$\hbar\omega_+ \approx -\epsilon_b + g_1\alpha \quad (29)$$

Thus,  $c = g_1\alpha$ . Since if  $P$  decreases then  $\alpha$  increases, it implies that if  $P$  decreases then the intercept  $c$  increases, and vice versa.

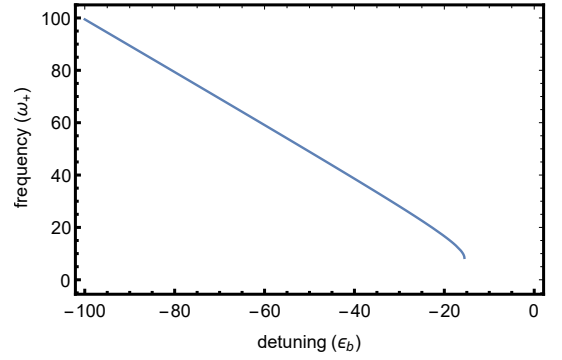


FIG. 15.  $\omega$  vs.  $\epsilon_b$  plot for  ${}^6\text{Li}$  (narrow resonance width) at  $P = 0.5$  for  $\epsilon_b > 0$  of PS state in 1D.

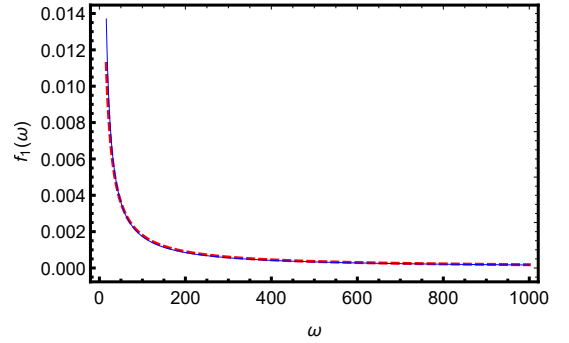


FIG. 16. Plot of  $f_1(\omega)$  denoted by blue solid line and its nearest function denoted by red dashed line vs.  $\omega$

### 2. Variation of slope ( $b$ ) with fractional imbalance ( $P$ )

The slope of the  $\omega$  vs.  $\epsilon_b$  curve, as per Eq. (27) is

$$b = \frac{d\omega_{\pm}}{d\epsilon_b} = -\frac{1}{2\hbar} \pm \frac{1}{2\hbar} \frac{\epsilon_b + g_1\alpha}{\sqrt{(\epsilon_b - \alpha g_1)^2 - 4\alpha(g_2^2 - \epsilon_b g_1)}} \quad (30)$$

We consider the non-trivial branch always, i.e., for  $\epsilon_b > 0$ ,  $b$  is calculated using  $\omega_-$ ; while for  $\epsilon_b < 0$ ,  $b$  is calculated using  $\omega_+$ . Accordingly,  $b$  vs.  $\alpha$  is plotted in Fig. 17. It shows that  $b$  increases linearly with  $\alpha$  when other parameters are held constant. Thus, if  $P$  decreases then  $b$  increases. This can explain the traits shown in Figs. 12, 13, and 14.

It is to be noted that Eq. 20 and the linearized form Eq. 23 imply that the slope ( $b$ ) of the  $\omega$  vs.  $\epsilon_b$  line accounts for the detuning-dependent (i.e., the magnetic field-dependent) contribution to the oscillation frequency, and the intercept ( $c$ ) accounts for the detuning-independent (i.e., the magnetic field-independent) contribution. Therefore, factors like (i) the amount of population imbalance present, and (ii) the nature of the pairing are reflected in the value of  $c$ . This is why the value of  $c$  changes appreciably if (i)  $P$  is varied, or (ii) one considers different phases but with the same amount of population imbalance.

On the other hand,  $b = \frac{\partial\omega}{\partial\epsilon_b}$  captures the detuning dependence of  $\omega$ . Therefore,  $b$  changes by a minimal amount if

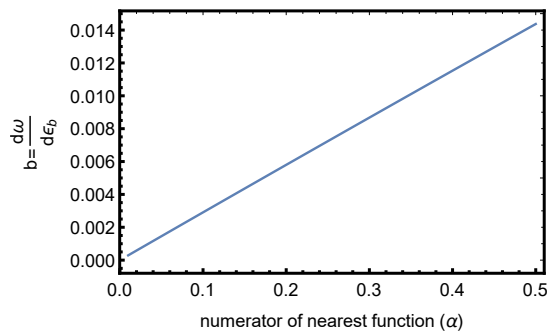


FIG. 17.  $b$  vs.  $\alpha$  plot for  $\epsilon_b < 0$

either the population imbalance or the pairing phase is altered.

### C. Physical significance for order of $b$ and $c$ in various phases

We observe that  $|c_{BP1}| > |c_{BP2}| > |c_{FFLO}| > |c_{PS}|$  as shown in Figs 9 - 11. This is because, when the bosons accumulate near  $k = 0$ , they form a more robust BEC, with less fluctuation. The PS state, which has bosons arranged in a region encircling  $k = 0$  thus has the lowest  $\omega$  value. Between BP2 and BP1, the BP1 phase has more atoms pushed away from the origin in  $k$ -space and is the least robust phase among all with the highest  $\omega$  value. FFLO state would be somewhere in between, depending on the value of  $P$ , as its structure is asymmetric and the amount of its skewness is governed by  $P$ .

We also observe that  $|b_{BP1}| > |b_{BP2}| > |b_{FFLO}| > |b_{PS}|$  as shown in Figs. 12 - 14. This is owing to the fact that when the bosons are concentrated near  $k = 0$ ,  $\omega$  changes by a small amount even if the detuning is changed. On the other hand, for phases that has bosons occupying higher  $k$ -values, the change in  $\omega$  would be greater for same amount of change in the detuning, as the BEC itself is less stable now.

The relative change in intercept, as shown in Fig. 11 is, however,  $\approx 10\%$  which can be well captured from experimental data. From Fig. 14, we obtain that the relative variation of the slope across the novel phases is  $\approx 0.001\%$  of the minimum value, which would be difficult to measure in experiments. This, again, is expected because the change in the momentum space structure directly influences  $c$ , as discussed in [Ref]. Thus, in order to differentiate between the exotic phases effectively, using the intercept data would be more suitable.

## VII. DISCUSSION

In this work, we theoretically studied the dynamics of the population-imbalanced ultracold fermions in an optical lattice. Considering a Feshbach coupling that enables the fermionic atoms to form bosonic molecules, we showed that beyond a small threshold value of the Feshbach detuning, the dynamics of the condensate fraction are always periodic. This implies that the oscillation is not just a small “fluctuation”,

rather, it is embedded in the mean-field description of the system itself: the periodic dynamics is sustained throughout the course of time. This result is independent of the amount of imbalance present in the system, as well as of the pairing structure.

In particular, we considered different pairing structures that arise in population-imbalanced fermionic systems, viz., Breached Pair (BP1 and BP2), Phase Separation (PS), Fulde-Ferrel-Larkin-Ovchinnikov (FFLO). Using the exact values of the Feshbach-resonance parameters of  ${}^6\text{Li}$  and  ${}^{40}\text{K}$ , we calculated the oscillation frequencies of the condensate fraction for each of these phases, and in different dimensions. The result is presented in the form of frequency ( $\omega$ ) versus Feshbach detuning ( $\epsilon_b$ ) plots. Again, we observed that neither the nature of the pairing (i.e., whether it is BP1/ BP2 /PS /FFLO) nor the choice of the atoms (e.g.,  ${}^6\text{Li}$  or  ${}^{40}\text{K}$ ), dimensionality (1, 2 or 3 dimensions) affects the overall qualitative description: The  $\omega$  vs.  $\epsilon_b$  curve always shows a straight-line like behaviour. This also implies that the dynamics of the population-imbalanced system in an optical lattice is markedly different from that in a harmonic trap/ homogeneous system [53].

The equation of the  $\omega$  vs.  $\epsilon_b$  straight line is dependent on the dimension of the system, the nature of the pairing, and most importantly, the amount of imbalance present. Thus, the slope and intercept of this line can provide interesting insight into the momentum-space structures of the different phases. The amount of imbalance can be deduced for a certain structure from the slope of this line if the slope/ intercept is known for the same system at some other fixed imbalance values. Useful information can also be gathered about the pairing structures, as both the slope and the intercept follow a specific sequence in terms of the exotic phases being present.

## VIII. ACKNOWLEDGEMENT

AM would like to acknowledge University Grants Commission (UGC), Govt. of India for financial support (Student ID: 201610064840). RD would like to acknowledge Science and Engineering Research Board (SERB), Dept. of Science and Technology, Govt. of India for providing support under the CRG scheme (CRG/2022/007312).

## AUTHOR CONTRIBUTION STATEMENT

Both the authors are involved in all stages of this work.

## DATA AVAILABILITY STATEMENT

All the data obtained from analytical/ numerical calculations have been presented in the forms of graphical plots. Some additional data are presented as tables in the Appendix.

---

\* [avinaba.mukherjee@rediffmail.com](mailto:avinaba.mukherjee@rediffmail.com)

† [rdphy@caluniv.ac.in](mailto:rdphy@caluniv.ac.in)

- [1] A. O. Koetsier, D. B. M. Dickerscheid, H. T. C. Stoof, Phys. Rev. A **74**, 033621 (2006)
- [2] E. Zhao and A. Paramekanti, Phys. Rev. Lett **97**, 230404 (2006)
- [3] A. Amaricci, A. Privitera and M. Capone, Phys. Rev. A **89**, 053604 (2014)
- [4] Z. Shen, L. Radzihovsky, and V. Gurarie, Phys. Rev. Lett **109**, 245302 (2012)
- [5] J. K. Chin, D. E. Miller, Y. Liu, C. Stan, W. Setiawan, C. Sanner, K. Xu and W. Ketterle, Nature **443**, 961 (2006)
- [6] W. V. Liu and F. Wilczek, Phys. Rev. Lett. **90**, 047002 (2003)
- [7] P. F. Bedaque, H. Caldas, and G. Rupak, Phys. Rev. Lett. **91**, 247002 (2003)
- [8] S-T. Wu and S. Yip, Phys. Rev. A **67**, 053603 (2003)
- [9] H. Caldas, C. W. Morais and A. L. Mota, Phys. Rev. D **72**, 045008 (2005)
- [10] R. Dasgupta, Phys. Rev. A **80**, 063623 (2009)
- [11] B. Deb, A. Mishra, H. Mishra, and P. K. Panigrahi, Physical Review A, **70**, 011604 (2004)
- [12] P. Zou, L. He, X. -J. Liu, and H. Hu, Phys. Rev. A **97**, 043616 (2018)
- [13] M. Karmakar, S. Roy, S. Mukherjee, and R. Narayanan, Phys. Rev. Research **4** 043159 (2022)
- [14] W. V. Liu, arXiv: 2109. 02208v2, 2022
- [15] D. E. Sheehy and L. Radzihovsky, Ann. Phys. **322**, 1790 (2007)
- [16] D. E. Sheehy and L. Radzihovsky, Phys. Rev. Lett. **96**, 060401 (2006)
- [17] Y. Shin, M. W. Zwierlein, C. H. Schunck, A. Schirotzek and W. Ketterle, Phys. Rev. Lett. **97**, 030401 (2006)
- [18] P. Fulde, R. A. Ferrel, Phys. Rev. A, **135**, 550, (1964)
- [19] A. I. Larkin, Yu. N. Ovchinnikov, Sov. Phys. JETP **20**, (1965)
- [20] T. Mizushima, K. Machida, and M. Ichioka, Phys. Rev. Lett. **94**, 060404 (2005)
- [21] O. K. Diessel, J. Von Milezewski, A. Christianen, and R. Schmidt, arXiv: 2209, 11758 (2022)
- [22] E. Vitali, P. Rosenberg, S. Zhang, Phys. Rev. Lett **128**, 203201 (2022)
- [23] T. Kawamura, R. Hanai, D. Kagamihara, D. Inotani, and Y. Ohashi, Phys. Rev. A **101**, 013602 (2020)
- [24] D. C. W. Foo, and G. J. Conduit, Phys. Rev. A **100**, 063602 (2019)
- [25] C. Gross and I. Bloch, Science **357**, 995 (2017)
- [26] S. Schmid, G. Thalhammer, K. Winkler, F. Lang, and J. H. Denschlag, New J. Phys. **8**, 159 (2006)
- [27] M. Aidelsburger, M. Atala, M. Lohse, J. T. Barreiro, B. Paredes and I. Bloch, Phys. Rev. Lett. **111**, 185301 (2013)
- [28] S. Rosi, A. Bernard, N. Fabbri, L. Fallani, C. Fort, M. Inguscio, T. Calarco and S. Montangero, Phys. Rev. A **88**, 021601 (2013)
- [29] A. Rosch, D. Rasch, B. Binz, and M. Vojta, Phys. Rev. Lett. **101**, 265301 (2008)
- [30] W. Hofstetter, J. I. Cirac, P. Zoller, E. Demler, M. D. Lukin, Phys. Rev. Lett **89**, 220407 (2002)
- [31] T. Paananen, T. K. Koponen, P. Törmä and J. P. Martikainen, Phys. Rev. A **77**, 053602, (2008)
- [32] A. Kujawa, R. Micnas, Acta Phys. Pol. A **114**, 43 (2008)
- [33] T. K. Koponen, T. Paananen, J.-P. Martikainen and P. Törmä, PRL **99**, 120403 (2007)
- [34] M. Karmakar, P. Majumdar, Phys. Rev. A **93**, 053609 (2016)
- [35] T. Koponen, J. Kinnunen, J-P. Martikainen, L. M. Jensen and P. Törmä, New J. Phys. **8**, 179 (2006)
- [36] I. Zapata, B. Wunsch, N. T. Zinner and E. Demler, Phys. Rev. Lett **105**, 095301 (2010)
- [37] A. Cichy, K.J. Kapcia, A. Ptok, Sci. Rep. **9**, 6719 (2019)
- [38] Theja N. De Silva Phys. Rev. A **91**, 053627 (2015)
- [39] J. Wang, L. Zhang, Y. Yu, C. Lee, and Q. Chen, Phys. Rev. A **101**, 053617 (2020)
- [40] J. Wang, L. Sun, Q. Zhang, L. Zhang, Y. Yu, C. Lee, and Q. Chen, Phys. Rev. A **101**, 053618 (2020)
- [41] M. O. J. Heikkinen and P. Törmä, Phys. Rev. A **83**, 053630 (2011)
- [42] J. P. A. Devreese, S. N. Klimin, and J. Tempere, Phys. Rev. A **83**, 013606 (2011)
- [43] J. P. A. Devreese, M. Wouters and J. Tempere, Phys. Rev. A **84**, 043623 (2011)
- [44] J. P. A. Devreese, S. Klimin, M. Wouters, and J. Tempere, Mod. Phys. Lett. B **26**, 1230014 (2012)
- [45] E. Altman, E. Demler, and M. D. Lukin, Phys. Rev. A **70**, 013603 (2004).
- [46] A. Lüscher, R. M. Noack, and A. M. Läuchli, Phys. Rev. A **78**, 013637 (2008).

- [47] D. Pećak and T. Sowiański, *Phys. Rev. Research*, **2**, 012077 (2020).
- [48] A. Korolyuk, F. Massel, and P. Törmä, *Phys. Rev. Lett.* **104**, 236402 (2010).
- [49] M. Singh and G. Orso, *Phys. Rev. Research*, **2**, 023148 (2020).
- [50] W. Yi and L.-M. Duan, *Phys. Rev. Lett.* **97**, 120401 (2006).
- [51] J. Kajala, F. Massel, and P. Törmä, *Phys. Rev. A* **84**, 041601(R) (2011).
- [52] L. Zhou, K. Zhang, B. Zhu, Y. Li and W. Zhang, *Physics Letters A* **376** (2012).
- [53] R. Dasgupta, J. K. Bhattacharjee, *The European Physical journal B* **94.2** (2021) : 1-14
- [54] S. Trotzky, P. Cheinet, S. Fölling, M. Feld, U. Schnorrberger, A. M. Rey, A. Polkovnikov, E. A. Demler, M. D. Lukin and I. Bloch, 2008, *Science* **319** 295-299
- [55] D. Hu, L. Niu, B. Yang, X. Chen, B. Wu, H. Xiong, and X. Zhou, *Phys. Rev. A* **92**, 043614 (2015)
- [56] Z. Wang, B. Yang, D. Hu, X. Chen, H. Xiong, B. Wu and X. Zhou, *Phys. Rev. A* **94**, 033624 (2016)
- [57] P. Kettmann, S. Hannibal, M. D. Croitoru, V. M. Axt, and T. Kuhn, *Phys. Rev. A* **96**, 033618 (2017)
- [58] A. Recati, and F. Piazza, *Phys. Rev. B* **99**, 064505 (2019)
- [59] E. A. Yuzbashyan, M. D. Zero, V. Gurarie, and M. S. Foster, *Phys. Rev. A* **91**, 033628 (2015)
- [60] J. Tokimoto, S. Tsuchiya, and T. Nikuni, *J. Phys. Soc. Jpn.* **88**, 023601 (2019)
- [61] L. Salasnich, *Condens. Matter* **2**, 22 (2017)
- [62] G. Lyu, K-T. Xi, S. Yoon, Q. Chen, and G. Watanabe, *Phys. Rev. A* **107**, 02332 (2023)
- [63] D. Phan, and A. V. Chubukov, *Phys. Rev. B* **107**, 134519 (2023)
- [64] S. M-Garot, G. Pettini, and M. Modugno, *Phys. Rev. A* **98**, 043624 (2018)
- [65] B. Sun, and M. S. Pindzola 2010 *J. Phys. B: At. Mol. Opt. Phys.* **43**, 055301
- [66] R. Combescot, M. Yu. Kagon, and S. Stringari, *Phys. Rev. A* **74**, 042717 (2006)
- [67] F. S. Cataliotti, S. Burger, C. Fort, P. Maddaloni, F. Minardi, A. Trombettoni, A. Smerzi, and M. Inguscio, 2001, *Science* **293**, 843
- [68] Y.-A. Chen, S. Nascimbéne, M. Aidelsburger, M. Atala, S. Trotzky, and I. Bloch, *Phys. Rev. Lett* **107**, 210405 (2011)
- [69] G. Kordas, D. Witthaut, and S. Wimberger, *Ann. Phys. (Berlin)* **527**, 619 (2015)
- [70] F. Trimborn, D. Witthaut, and S. Wimberger, *J. Phys. B: At., Mol. Opt. Phys.* **41**, 171001 (2008)
- [71] F. Trimborn, D. Witthaut, H. Hennig, G. Kordas, T. Geisel and S. Wimberger, *Eur. Phys. J. D* **63**, 63 (2011)
- [72] A. Vardi, V. A. Yurovsky, and J. R. Anglin **64**, 063611 (2001)
- [73] A. Vardi and J. R. Anglin, **86**, 568 (2001)
- [74] G. Kordas, D. Witthaut, P. Buonsante, A. Vezzani, R. Burioni, A. I. Karanikas, and S. Wimberger, *Eur. Phys. J: spec. Top.* **224**, 2127 (2015)
- [75] F. Dalfovo, S. Giorgini, L. P. Pitaevskii, and S. Stringari, *Rev. Mod. Phys.* **71**, 3, 1999
- [76] T. Rom, Th. Best, D. Van Oosten, U. Schneider, S. Fölling, B. Parades, and I. Bloch, *Nature* **444**, 733-736 (2006)
- [77] M. Kohl, H. Moritz, T. Stoferle, K. Gunter, T. Esslinger, *Phys. Rev. Lett.* **94**, 080403 (2005)
- [78] S. Ramanan, T. Mishra, M. S. Luthra, R. V. Pai, and B. P. Das. *Phys. Rev. A* **79**, 013625 (2009)
- [79] T. Stoferle, H. Moritz, C. Schori, M. Kohl, and T. Esslinger *Phys. Rev. Lett.* **92**, 130403 (2004)
- [80] I. Jimenez-Garcia, R. L. Compton, Y. - J. Lin, W. D. Phillips, J. V. Porto, and I. B. Spielman *Phys. Rev. Lett* **105**, 110401 (2010)
- [81] A. Isacsson, and S. M. Girvin, 2005, *Phys. Rev. A* **72**, 053604
- [82] Y. Matsunda, H. Shimahara, *J. Phys. Soc. Jph* **76**, 051005 (2007)
- [83] Carlos AR. Sa de Melo, *Phys. Today* **61**. 10 (2008)
- [84] C. Kollath, A. Iucci, T. Giamarchi, W. Hofstetter, and U. Schollwöck, *Phys. Rev. Lett* **97**, 050402 (2006)
- [85] A.-M. Dare, L. Raymond, G. Albinet, and A. -M. S. Tremblay, *Phys. Rev. B* **76**, 064402 (2007)
- [86] R. Sensarma, D. Pekker, M. D. Lukin, and E. Demler, *Phys. Rev. Lett.* **103**, 035303 (2009)
- [87] H. Pichler, J. Schachenmayer, A. J. Daley, and P. Zoller, *Phys. Rev. A* **87**, 033606 (2013)
- [88] M. Lubasch, F. Mintert, and S. Wimberger, *Phys. Rev. A* **84**, 063615 (2011)
- [89] J.-W. Huo, F.-C. Zhang, W. Chen, M. Troyler, and U. Schollwöck, *Phys. Rev. A* **84**, 043608 (2011)
- [90] F. Illuminati and A. Albus, *Phys. Rev. Lett* **93**, 090406 (2004)
- [91] Z. Xu, S. Chiesa, S. Yang, S. -Q. Su, D. E. Sheenhy, J. Moreno, R. T. Scalettar and M. Jarrell, *Phys. Rev. A* **84**, 021607 (2011)

- [92] Chartkunchand, K. (2006). Ultracold Atoms in Optical Lattices. (Doctoral dissertation, University of Nevada, Reno)
- [93] J. A. Scaramazza, B. Kain and H. Y. Ling, *The European Physical Journal D* **70**, 147 (2016)
- [94] T. Kohler, K. Goral and P. S. Julienne, *Rev. Mod. Phys.* **78**, 1311 (2006)
- [95] I. Bloch, J. Dalibard and W. Zwerger, *Rev. Mod. Phys.* **80**, 885 (2008)
- [96] M. Holland, S. J. J. M. F. Kokkelmans, M. L. Chiofalo and R. Walser, *Phys. Rev. Lett* **87**, 120406, (2001)
- [97] C. J. Pethick, and H. Smith, *Bose-Einstein Condensation in Dilute Gases* (Cambridge University Press, New York, 2008) 2nd Edition
- [98] L. Pitaevskii, and S. Stringari, *Bose-Einstein Condensation and Superfluidity* (Oxford Science Publications, United Kingdom, 2015) International Series of Monographs on Physics-164



### Appendix A: Calculation of parameters for ${}^6\text{Li}$ and ${}^{40}\text{K}$

In this section, we compute the  $g_1$  and  $g_2$  values for  ${}^6\text{Li}$  and  ${}^{40}\text{K}$  corresponding to different amounts of fractional imbalance and dimension for  ${}^6\text{Li}$  and  ${}^{40}\text{K}$  sample. Building elements of  $g_1$  and  $g_2$  for both  ${}^6\text{Li}$  and  ${}^{40}\text{K}$  has been shown in Table [I] in the page of tables. Table II, Table III and Table IV are given on the page of the table for various dimensions of system parameters.

TABLE I. Building elements of  $g_1$  and  $g_2$  [94]

Species	resonance width ( $\Delta B$ )	resonance position ( $B_0$ )	background scattering length ( $a_{bg}$ )
${}^6\text{Li}$	0.1 G	543.25 G	$59a_0$
${}^6\text{Li}$	-300 G	834.149 G	$-1450a_0$
${}^{40}\text{K}$	7.8 G	202.10 G	$174a_0$
${}^{40}\text{K}$	9.7 G	224.21 G	$174a_0$

TABLE II. System parameters for 1D

Species	resonance width ( $\Delta B$ )	t (set $0.065E_r^F = 1$ )	$g_1$ (set $0.065E_r^F = 1$ )	$g_2$ (set $0.065E_r^F = 1$ )	$\hbar$
${}^6\text{Li}$	0.1 G	1	5.785	17.077	1
${}^6\text{Li}$	-300 G	1	-137.785	4566.969	1
${}^{40}\text{K}$	7.8 G	1	17.062	613.215	1
${}^{40}\text{K}$	9.7 G	1	17.062	683.862	1

TABLE III. System parameters for 2D

Species	resonance width ( $\Delta B$ )	t (set $0.065E_r^F = 1$ )	$g_1$ (set $0.065E_r^F = 1$ )	$g_2$ (set $0.065E_r^F = 1$ )	$\hbar$
${}^6\text{Li}$	0.1 G	1	3.6	13.477	1
${}^6\text{Li}$	-300 G	1	-85.738	3602.677	1
${}^{40}\text{K}$	7.8 G	1	10.615	483.723	1
${}^{40}\text{K}$	9.7 G	1	10.615	539.676	1

TABLE IV. System parameters for 3D

Species	resonance width ( $\Delta B$ )	t (set $0.065E_r^F = 1$ )	$g_1$ (set $0.065E_r^F = 1$ )	$g_2$ (set $0.065E_r^F = 1$ )	$\hbar$
${}^6\text{Li}$	0.1 G	1	2.246	10.631	1
${}^6\text{Li}$	-300 G	1	-53.369	2841.6	1
${}^{40}\text{K}$	7.8 G	1	6.6	381.738	1
${}^{40}\text{K}$	9.7 G	1	6.6	425.538	1

TABLE V. Range of detuning ( $\Delta\epsilon_b$ ) which generates an imaginary frequency solution in 1D

Phase	nearest function ( $f_1(\omega) = \frac{\alpha}{\hbar\omega}$ )	numerator of nearest function ( $\alpha$ )	$\Delta\epsilon_b$
PS	0.00421729	0.421729	40.372
FFLO	0.00421212	0.421212	40.328
BP2	0.004196	0.4196	40.284
BP1	0.00418503	0.418503	40.240

TABLE VI. Variation of nearest form of  $f_1(\omega)$  with fractional imbalance for PS state and  $\text{Li}^6$  sample in 1D

fractional imbalance (P)	paired region	actual form of $f_1(\omega = 16 \text{ to } 1000)$	numerator of nearest function( $\alpha$ )
0.1	$-\pi/2.4$ to $\pi/2.4$	$\frac{0.63662 \text{ArcTanh} \frac{-2.9924 - 0.748591\omega}{15.9999931 + (0.005242 - \omega)\omega}}{16 + (0.005242 - \omega)\omega}$	0.38
0.3	$-\pi/3$ to $\pi/3$	$\frac{0.63662 \text{ArcTanh} \frac{-1.796 - 0.450\omega}{15.999 + (0.0157 - \omega)\omega}}{15.999 + (0.016 - \omega)\omega}$	0.28
0.5	$-\pi/2$ to $\pi/2$	$\frac{0.63662 \text{ArcTanh} \frac{-1.06829 - 0.2679\omega}{15.9998 + (0.0262 - \omega)\omega}}{15.9998 + (0.0262 - \omega)\omega}$	0.18
0.7	$-\pi/7$ to $\pi/7$	$\frac{0.63662 \text{ArcTanh} \frac{-0.555 - 0.139\omega}{15.9997 + (0.036 - \omega)\omega}}{15.9997 + (0.036 - \omega)\omega}$	0.1
0.9	$-\pi/10$ to $\pi/10$	$\frac{0.63662 \text{ArcTanh} \frac{-0.16449 - 0.0413603\omega}{15.9995 + (0.046 - \omega)\omega}}{15.9995 + (0.046 - \omega)\omega}$	0.028